Protein Stability in a Natural Deep Eutectic Solvent: Preferential Hydration or Solvent Slaving?

Inês Gomes[a], Nuno Galamba[a,*]

[a] BioISI - Biosystems and Integrative Sciences Institute, Faculty of Sciences of the University of Lisbon, C8, Campo Grande, 1749-016 Lisbon, Portugal.

[*]Corresponding author: njgalamba@fc.ul.pt

Abstract

Deep eutectic solvents (DESs) emerged as potential alternative solvent media in multiple areas, including biomolecular (cryo)preservation. Herein, we studied the stability of a small protein (ubiquitin) in water and a betaine-glycerol-water (B:G:W) (1:2:ζ; ζ = 0, 1, 2, 5, 10) DES, through molecular dynamics. An AMBER-based model that accurately describes the density and shear viscosity of the DES is proposed. We find that water molecules are largely trapped in the solvent, precluding the formation of a full hydration layer, seemingly opposite to osmolytes' preferential exclusion/preferential hydration mechanism. Whereas the protein is stable in the DES, structural fluctuations are largely suppressed and only recovered upon sufficient hydration. This is explained by a solvent slaving mechanism where β-fluctuations are key, also explaining the non-monotonic folding of some proteins in aqueous DESs. A thermal stability enhancement in the DES is also observed, caused by a similar slowdown of the backbone torsional dynamics. Our results support a kinetic stabilization of the protein in the DES, whereas a possible thermodynamic stabilization does not follow a preferential hydration or water entrapment mechanism.

Introduction

Deep eutectic solvents (DESs) are a class of green solvents with a wide range of potential applications[1–4]. Amongst the latter, DESs have been increasingly explored as sustainable media in biochemical processes, in particular biocatalysis[5–28]. Additionally, DESs might be a suitable media for the (cryo)preservation[29] of other vulnerable biomolecules (e.g., DNA and RNA), cells[30–32] (e.g., stem cell storage), or even organs for transplantation.

DESs are mixtures formed by a hydrogen bond (HB) donor and an HB acceptor, characterized by a depression of the melting point relative to its components[1–3]. While sharing several properties with room temperature ionic liquids, notably, negligible vapor pressures, nonflammability, and thermal stability, they have, in general, various advantages, including, biodegradability, reduced cost, and low toxicity[1].

DESs are commonly exceedingly viscous fluids and water is normally used to reduce their viscosity for specific applications[2]. On the other hand, a fundamental issue concerns the amount of water essential to protect biomolecular structure and function[6,16,17,19,20,24]. Living organisms developed protective mechanisms to cope with dehydration, freezing, and hypoxia, which include the synthesis of protective osmolytes (e.g., trehalose, trimethylamine N-oxide, betaine, glycerol). Other osmolytes, such as urea, are protein denaturants[33,34], although its destabilizing effect can be suppressed when mixed with other osmolytes and in DESs[5,7,8]. Since many components of natural DESs (so-called NADESs) are osmolytes, it has been hypothesized that NADES could be "the third liquid phase in organisms in which certain biosynthetic steps or storage of products may occur"[35].

Osmolyte protein stabilization has been associated with a preferential-exclusion/preferential-hydration mechanism, in which osmolytes are excluded from the proteins' surface[29,36–41]. Osmolyte exclusion is believed to shift the protein folded-unfolded equilibrium (F $\rightleftharpoons$ U) toward the F state by increasing the free energy of the U state[42]. From a molecular perspective such a shift has been connected with an increase of the solvent (water) accessible surface area (SASA) of proteins upon preferential hydration[29,41]. Alternative explanations have, however, been put forward[29].

A comprehensive understanding of the relationship between the biomolecular protection mechanisms of NADESs and the protective mechanism of osmolytes, intracellular crowding effects, and the importance of water, remains, however, incomplete.

Herein, we aimed at gaining insight into the role of water and the molecular source of the putative enhanced thermal stability of a prototypical globular protein in a betaine-based NADES. For this purpose, we studied ubiquitin (UBQ) in a Betaine:Glycerol:Water (B:G:W) (1:2:ζ; ζ = 0, 1, 2, 5, 10) DES through molecular dynamics simulations at temperatures ranging from 298 K to 450 K.

Betaine (aka trimethylglycine) is a naturally occurring osmolyte present in several organisms, including animals and plants. Glycerol is also a natural osmolyte well-known for its cryoprotective

properties. A B:G:W DES has been shown to be a suitable media for several proteins[16,23,25]. UBQ is a small, highly compact, 76-amino acid protein, highly conserved across eukaryotes. The protein has approximately 87% of the polypeptide chain involved in hydrogen-bonded secondary structure[43]. The latter includes 3.5 turns of α-helix, a short segment of 3_{10}-helix, a mixed β-sheet with five strands, and seven reverse turns[43].

The remaining of the article is organized as follows: The methods used in this work are described in section II. In section III we discuss the protein's structure and torsional dynamics dependence of the viscosity, hydration, and water's orientational dynamics, in light of a solvent slaving model. Next, we discuss the thermal stability of the protein in the DES in the absence of water. We end with conclusions in Section IV.

II. Methods

A. Force Field

The starting configuration of UBQ was obtained from the crystal structure (PDB Code: 1UBQ[44]). UBQ was described by the AMBER99sb force field[45] (FF) whereas water was described by the TIP4P-Ew[46] model. For betaine (Bet) and glycerol (Gly), generalized AMBER FF (GAFF)[47] parameters were derived (see **Fig. S1** and **Tables S1** and **S2**). The geometry of Bet and Gly was optimized at the B3LYP[48]/6-31G* theoretical level and RESP[49] charges were computed at the HF/6-31G* level[47]. The latter calculations were performed with the program GAUSSIAN 09[50]. However, the density and viscosity were found to be significantly larger than the experimental values for a B:G (2:1) DES (see **Table S3**). To improve the FF for betaine and glycerol the RESP charges were first scaled by a factor $\lambda_Q < 1$, while the remaining parameters were kept unchanged. **Figure S2** shows that the density decays very slowly with the decrease of λ_Q, and, thus, with the magnitude of the atomic charges. The viscosity, in turn, varies significantly with the electrostatic charges, exhibiting a rapid decrease. As a consequence, there is no λ_Q for which the density and viscosity are concomitantly well described. This means that GAFF cannot accurately model the DES simply by scaling the atomic charges. The overestimation of the density even at low λ_Q suggests that the short-range Lennard-Jones (LJ) repulsions (i.e., Pauli repulsion) are too soft, allowing forming structures too compact. From an intermolecular forces' perspective such repulsions in the DES (i.e., Bet-Bet, Bet-Gly, and Gly-Gly) should be different from those between Bet-OW and Gly-OW for which the GAFF model is expected to be valid. Furthermore, polarization and charge transfer effects, accounted in an average way, should be significantly different in these environments and the FF must be reweighted to reflect such differences and prevent the formation of a solid (high λ_Q) or a high density pseudo-liquid (low λ_Q). To account for these, we introduced a second parameter, ($\lambda_\sigma > 1$), to scale the σ of the LJ potential; the σ is the distance at which the LJ pair potential energy is zero and is related to the distance, r_0, at which

the potential has a minimum (i.e., $\partial u^{LJ}(r)/\partial r = 0$), by $r_0 = 2^{1/6}\sigma$. Whereas the well-depth of the LJ potential could be used instead, varying the van der Waals radius to reproduce the experimental density is a more intuitive approach.

The introduction of a second parameter, however, means that multiple combinations are possible, where both properties are well described. Here, we followed a simple approach, based on preliminary calculations, that showed that the increase of σ results in a rapid decrease of ρ and a slow decrease of η, opposite to λ_Q. **Figure S2(b)** shows that the decrease of the density with λ_σ is more pronounced than with $1/\lambda_Q$ by nearly an order of magnitude. Thus, we defined λ_Q as to give a viscosity above the experimental value and then varied λ_σ as to give ρ and η close to the experimental data. **Figure S2(d)** shows the λ_σ dependence of the shear viscosity of the DES. This approach allowed placing most of the FF recalibration upon λ_Q while minimizing the perturbation of the σ. This resulted in the following scaling parameters: $\lambda_Q = 0.92$ and $\lambda_\sigma = 1.03$, that is, an 8% reduction of the atomic charges and a 3% increase of the atomic σ. This FF, hereinafter referred to as GAFF-opt, overestimates the experimental density (1.216 g·cm^{-3}) by 0.58 % whereas the viscosity is underestimated by ~7% (see **Table 1**). **Table 1** also compares the density, viscosity, and self-diffusion coefficients with those estimated through another FF (OPLS-aa) by our group[51]. Interestingly, the onset of the OPLS-aa radial distribution functions (RDFs) is still lower than that for the GAFF-opt, with the exception of the Gly-Gly RDF for which the onset is the same (see **Fig. S3**). Further, a good agreement is observed among the RDFs for the two FFs, with the GAFF-opt giving slightly lower coordination numbers.

Table 1 – Density, ρ, viscosity, η, and self-diffusion, D, of the components, for Bet:Gly (1:2). The results of this work are compared with those from experiments and another FF (OPLS-aa) previously reported by our group.

Exp./MD	ρ (g·cm^{-3})	η (mPa·s)	D_B (10^{-8} cm^{2}s^{-1})	D_G (10^{-8} cm^{2}s^{-1})
Experimental	1.216	1528	-	-
OPLS-aa[51]	1.185	1536±222	0.63±0.05	1.0±0.05
GAFF-opt[a]	1.223	1417±20	0.83±0.05	1.19±0.05

[a] This work.

B. Molecular Dynamics

The MD simulations were carried out in the isothermal-isobaric (*NpT*) ensemble in a cubic box with periodic boundary conditions, with the program GROMACS[52]. The T and p were controlled with the thermostat of Bussi *et al.*[53] and the Parrinello-Rahman barostat[54]. Electrostatic interactions were computed via the particle-mesh Ewald (PME) method[55]. A cut-off of 1 nm was used for non-bonded van der Waals and the PME real space electrostatic interactions. Heavy atom-hydrogen covalent bonds were constrained with the LINCS algorithm[56].

The MD simulations of the DES (B:G) to assess its density and viscosity at different λ_Q and λ_σ, in the absence of water, were performed for 128 molecules of betaine (Bet) and 256 molecules of glycerol (Gly). These trajectories were propagated for 1 μs to calculate the viscosity with a reasonable accuracy.

MD simulations of betaine-glycerol-water (B:G:W) (1:2:ζ; ζ = 1, 2, 5 and 10) at 298 K and 0.1 MPa with the GAFF-opt (i.e., λ_Q = 0.92 and λ_σ = 1.03) were then performed for 450 molecules of Bet, 900 molecules Gly, and 450, 900, 2250, and 4500 water molecules, respectively, corresponding to the following water molar percentages (mol %) 25, 40, 62.5, 76.9, and weight percentages (wt %), 5.6, 11.3, 28.2, and 56.4. These simulations were performed primarily to validate the FF when water is added to the system. A recent study by our group[51] showed that above ζ = 7 (70 mol%; 56.4 wt%) a major structural transformation occurs in this DES, with the complete disruption of the second Bet-Gly solvation layer; a similar transformation in passing from ζ = 5 to 10 was also observed here (see **Fig. S4**). The length of these trajectories ranged between 1 μs for ζ = 1 to 500 ns for ζ = 10.

MD of UBQ in the DES for ζ = 0, 1, 2, 5, and 10 were carried out at 298 K and 0.1 MPa to assess the role of water on the protein structure. The systems were first equilibrated in the *NpT* ensemble for 100 ns after a 100 ps simulation in the canonical (*NVT*) ensemble. The trajectories (five replicas for each system) were then propagated in the *NpT* ensemble for around 500 ns/replica.

To assess the thermal stability of UBQ in water and in the DES MD simulations (two replicas) at 373 K, 410 K, 425 K, and 450 K were performed. The MD in water above 373 K, were carried out in pressurized hot water to ensure water is liquid. Thus, the following *T* and *p*, were chosen: 373 K, 0.1 MPa (1 bar), 410 K, 425K, 0.5 MPa (5 bar), and 450 K, 1 MPa (10 bar). The trajectories were propagated for 1.9 μs after a 100 ns period for "equilibration". To assess the effect of pressure on protein structure, since proteins denaturate at high pressures, albeit in the 100 MPa (kbar) range[57,58], simulations in the DES at similar pressures were also performed. Further, MD in water at high temperatures and 0.1 MPa were alco carried out, for comparison purposes, in spite real water does not exist in the liquid state at these temperatures.

The equations of motion were solved with the Verlet leap-frog algorithm with a 1 fs time-step for the DESs (without UBQ) for every ζ and UBQ in the DESs and 2 fs for UBQ in water. MD of UBQ in water with a time-step of 1 fs were also carried out (replica 2) at every temperature, to discard any possible protein stability time-step dependence.

C. Structure and Transport Coefficients

The self-diffusion coefficients of the DESs' components were estimated through the Einstein relation[59],

$$D = \frac{1}{6}\lim_{t\to\infty}\frac{d}{dt}\left\langle \sum_{i=1}^{N} |r_i(t) - r_i(0)|^2 \right\rangle \quad (1)$$

where the < > indicate an ensemble average of the mean square displacement (MSD), $r_i(t)$ and $r_i(0)$ are the positions of the ith particle at time t and the origin, respectively, and D is the diffusion coefficient. For normal diffusion, the MSD grows linearly at long times, and D can be estimated from the slope of the MSD.

The shear viscosity, η, was calculated through integration of the stress (aka pressure) tensor time correlation function[60],

$$\eta = \frac{V}{10k_BT}\int_0^\infty \left\langle \sum_{\alpha\beta}^{9} P_{\alpha\beta}(0)P_{\alpha\beta}(t) \right\rangle dt \quad (2)$$

where $P_{\alpha\beta}$ is the symmetrized traceless portion of the stress tensor, $\sigma_{\alpha\beta}$, given by[61],

$$P_{\alpha\beta} = \frac{1}{2}\left(\sigma_{\alpha\beta} + \sigma_{\beta\alpha}\right) - \frac{1}{3}\delta_{\alpha\beta}\left(\sum_{\alpha}\sigma_{\alpha\alpha}\right) \quad (3)$$

$\delta_{\alpha\beta}$ is the Kronecker delta and there are six, out of the nine, distinct $P_{\alpha\beta}$ elements. This expression allows improving the statistics over the original Green-Kubo formula which involves the average over only the three different off-diagonal elements, $\sigma_{\alpha\beta} = \sigma_{\beta\alpha}$, of the stress tensor[59],

$$\eta = \frac{V}{3k_BT}\int_0^\infty \left\langle \sum_{\alpha\beta}^{3} \sigma_{\alpha\beta}(0)\sigma_{\alpha\beta}(t) \right\rangle dt \quad (4)$$

also used here for comparison purposes; no significant differences were found between the viscosity calculated with eqs (2) and (4). For the definition of the stress tensor elements for periodic systems treated with the Ewald or the particle-mesh Ewald methods see refs ([62–65]).

The secondary structure of UBQ was assessed with the program DSSP[66]. The torsional dynamics of the protein backbone was also assessed by calculating the ϕ (phi) and ψ (psi) time correlation functions. The dihedral time correlation function proposed by van der Spoel and Berendsen was adopted[67]. The latter is given by,

$$C_\alpha(t) = \left\langle \cos[\alpha(0)]\cos[\alpha(0+t)] + \sin[\alpha(t)]\sin[\alpha(0+t)] \right\rangle \quad (5)$$

in which $C_\alpha(t)$ reduces to the fundamental Pythagorean trigonometric identity at zero delay time, that is, $C_\alpha(0) = 1$, and where α = ϕ, ψ were assessed.

The orientational dynamics of water was also studied through the calculation of the orientational auto-correlation functions[68],

$$C_l(t) = P_l\left[\mathbf{u}_{\mathbf{r}_{OH}}(0)\cdot\mathbf{u}_{\mathbf{r}_{OH}}(t)\right] \quad (6)$$

where $\mathbf{u}_{\mathbf{r}_{OH}}$ is the intra-molecular OH unit vector and P_l is the l^{th} order Legendre polynomial (l = 1, 2,

and 3); results are reported for l = 2.

III. Results and Discussion

Figure 1 depicts the density, ρ, shear viscosity, η, self-diffusion coefficients, D, and the coordination numbers (CNs) obtained through integration of the respective RDFs up to the first minimum, for the (B:G:W) DES at the different water contents. The ρ, η, D and the CNs were fitted to the equation[51],

$$Z = Z_0 \exp[-a_z/(\zeta + b_z)] \quad (7)$$

where Z stands for either ρ, η, D, or CN, and Z_0, a_z, and b_z are property dependent empirical parameters; Eq. (7) was shown to accurately describe several properties, including ρ, D, and η, as well as structural parameters for a betaine-glycerol DES[51] and reline[69].

An excellent agreement with the experiments is found for the density whereas the viscosity is underestimated with the error decreasing with the water content. Additionally, a behavior similar to that found with an OPLS-aa force field[51] regarding the hydration of the different species is found, that is, a faster hydration of Bet, relative to Gly (**Fig. 1(d)**).

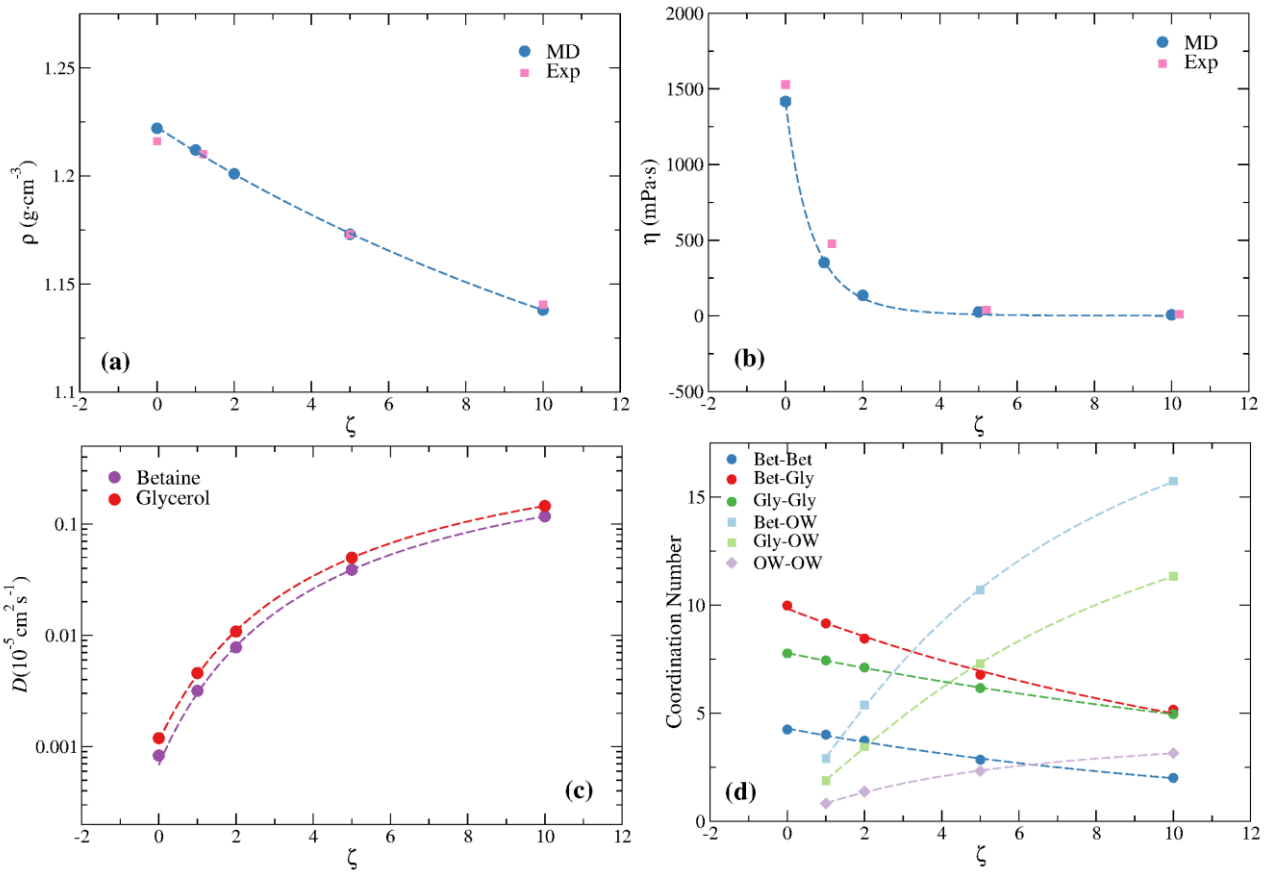

Figure 1 – Betaine-Glycerol-Water (B:G:W) (1:2:ζ; ζ = 0, 1, 2, 5, and 10) DES properties at 298 K and 0.1 MPa. **(a)** density, **(b)** shear viscosity, **(c)** self-diffusion coefficients of Bet and Gly, and **(d)** coordination numbers. Dashed lines are fits to eq. (7).

Figures 2a and 2b show, respectively, the radius of gyration, R_g, and the secondary structure of UBQ in the different solvents at 298 K and 0.1 MPa. A narrower R_g distribution is found for UBQ in the DES, relative to water, falling within the peak that corresponds to the more extended conformations of UBQ in water. Addition of water results in a broadening of R_g although a non-monotonic shift of the main peak is observed. At $\zeta \sim 5$ a significant broadening of the R_g distribution occurs and at $\zeta = 10$ a more similar distribution to that in water can be observed.

In spite of the differences of the R_g distribution a nearly indistinguishable secondary structure is observed in water and in the various DESs, independent of the water content, with 16% α-helix and ~31% β-sheet, in good agreement with the crystal structure[43,58]. The suppression of the R_g fluctuations and the nearly constant secondary structure suggests that the DES should mainly affect the dynamics of the protein. To understand how the addition of water may influence the dynamics of the protein, we assessed the fraction of water molecules in the DES and next to the protein. The latter are sometimes called "biological" water (or "bound" water) and are defined here as the water molecules within 5.5 Å of any heavy atom of the protein (see **Fig. 2c** and **2d)**.

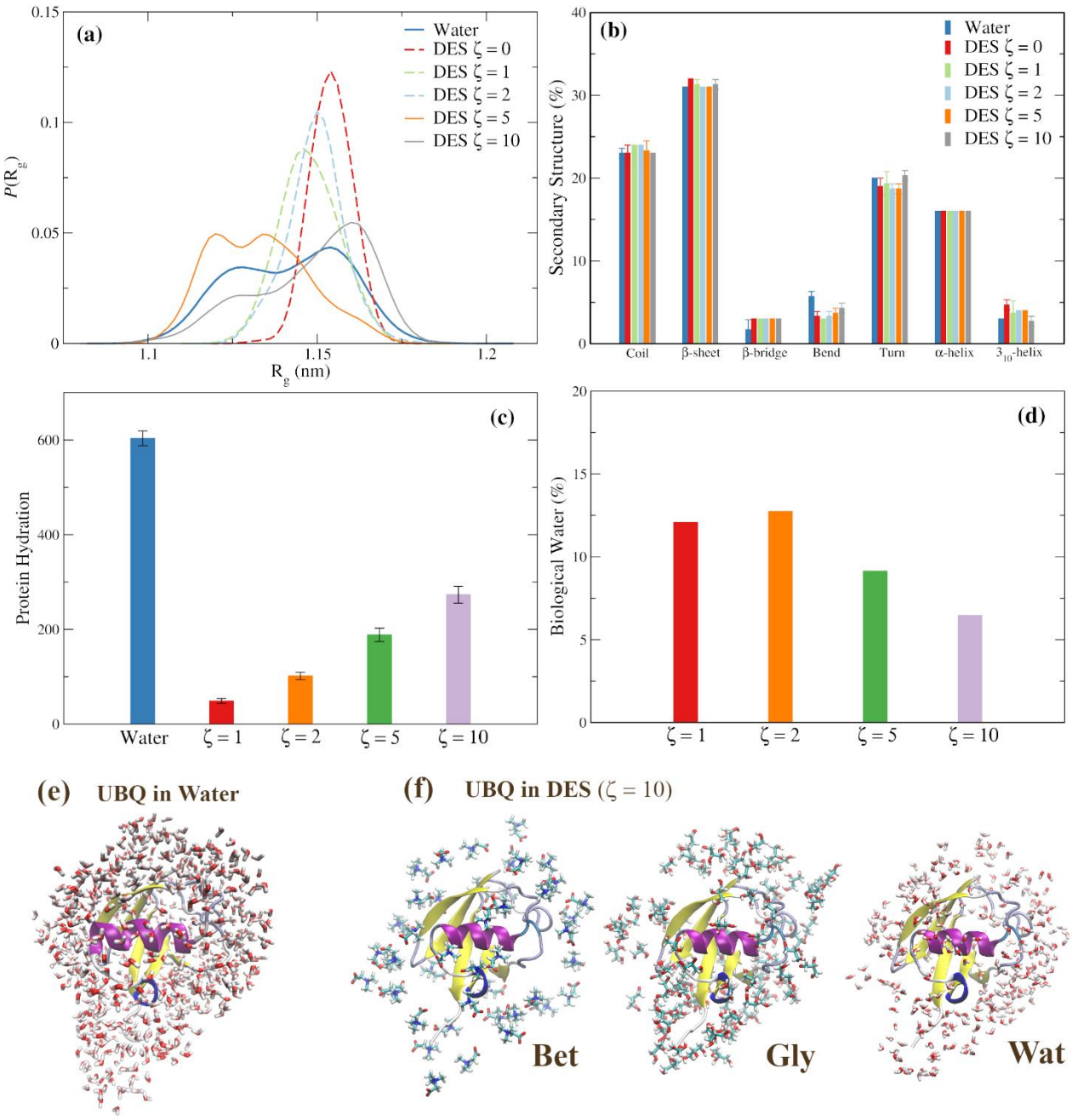

Figure 2 – **(a)** Radius of gyration distribution, **(b)** secondary structure, **(c)** hydration (absolute number), and **(d)** percentage of biological (or bound) water. The protein's hydration layer called here biological water (BW) was defined by the water molecules within a radial distance $r_{BW} < 5.5$ Å of any protein heavy atom; the latter encompasses the first hydration layer of most amino acid side chains; different definitions resulted in similar qualitative results. **(e)** and **(f)** show a MD snapshot with the number solvent molecules at a distance of 5.5 Å of any UBQ heavy atom in water and in the DES (ζ = 10), respectively.

Addition of water results in the appearance of a hydration layer around the protein. However, even at ζ = 10, UBQ's hydration layer is formed by less than half of the water molecules around the protein in water (see **Fig. 2c**). Furthermore, this represents less than 15% (less than 7.5% for ζ = 10) of the water in solution for every ζ (see **Fig. 2d**). Thus, water molecules are largely trapped in the solvent not exhibiting a clear preference for the protein surface, seemingly opposite to the preferential

exclusion/preferential hydration or water entrapment mechanisms in aqueous solutions of osmolytes (protein stabilizers)[29,38,39,41].

We now turn attention to the dynamics of the protein in water and in the DES, and the way water influences the protein dynamics. We analyzed the rotational dynamics around UBQ's backbone N-Cα and Cα-C bonds, in particular, the torsion (dihedral) angles ϕ (phi) and ψ (psi) time-correlation functions. Amongst the latter we focused on the dihedrals of the α-helix (amino acids 23-34), since unfolding seems to start at this segment as discussed below.

Figure 3 for C_ψ shows that the torsional dynamics undergoes a slowdown only recovered upon addition of sufficient water ($\zeta > 10$); a similar result is found for C_ϕ (**Fig. S5**). This is more visible in the terminal amino acids of the α-helix, in particular, Asp32, Lys33, and Glu34. Fitting the dihedral time correlation function of Asp32 (fastest decay function in water – see **Fig. 3**) to a two-term relation of the form[67,68],

$$C(t) = a + b\exp(-t/\tau) \tag{8}$$

where τ is a dihedral relaxation time, gives the following slowdown factors: $\tau_{DES(\zeta=0)}/\tau_{Wat} \sim 42$ and $\tau_{DES(\zeta=10)}/\tau_{Wat} \sim 12$ (see **Fig. S6(a)**). For Glu24, however, $\tau_{DES(\zeta=0)}/\tau_{Wat} \sim 1.5$. The reason is a much lower hydration difference between the backbone of Glu24 across the systems, as discussed below. We also tried other functional forms, including a stretched exponential, a biexponential, and the sum of a power law and exponential since eq. (8) does not fit equally well all the functions. A stretched exponential did not improve the fittings. The power law and exponential,

$$C(t) = a + ct^{\delta} + b\exp(-t/\tau) \tag{9}$$

provided the best fittings (see **Fig. S6(c)**). However, this function leads to ambiguities concerning the physical meaning of the power law exponent, δ, and the exponential decay constant, τ, since c is always negative, and for large water contents b can become negative and $a > 1$. For this reason, in what follows, eq.(8) is used to model the long time relaxation of the torsional time correlation functions.

The above slowdown factors can be interpreted within the kinetic framework of "protein slaving" in which solvent fluctuations or α-fluctuations and β-fluctuations (solvation shell coupled fluctuations) (in analogy with α- and β-fluctuations in glass forming fluids) limit the conformational substates of the protein[70–74]. We note that β-fluctuations can also be interpreted in terms of the solvent being slaved to protein interactions and excluded volume, known to slowdown the dynamics of "biological" or "bound" water.

Under the slaving model, large-scale motions occur through a large number of steps (*e.g.*, ϕ and ψ torsions) determined by the solvent fluctuations. These large-scale motions are involved both in protein folding and unfolding (discussed below), but slaving can be readily seen concerning

conformational fluctuations at room temperature where native UBQ is stable. This should, therefore, explain the slowdown of the torsional dynamics of the backbone of the α-helix of UBQ as well as the narrowing of the distribution of R_g.

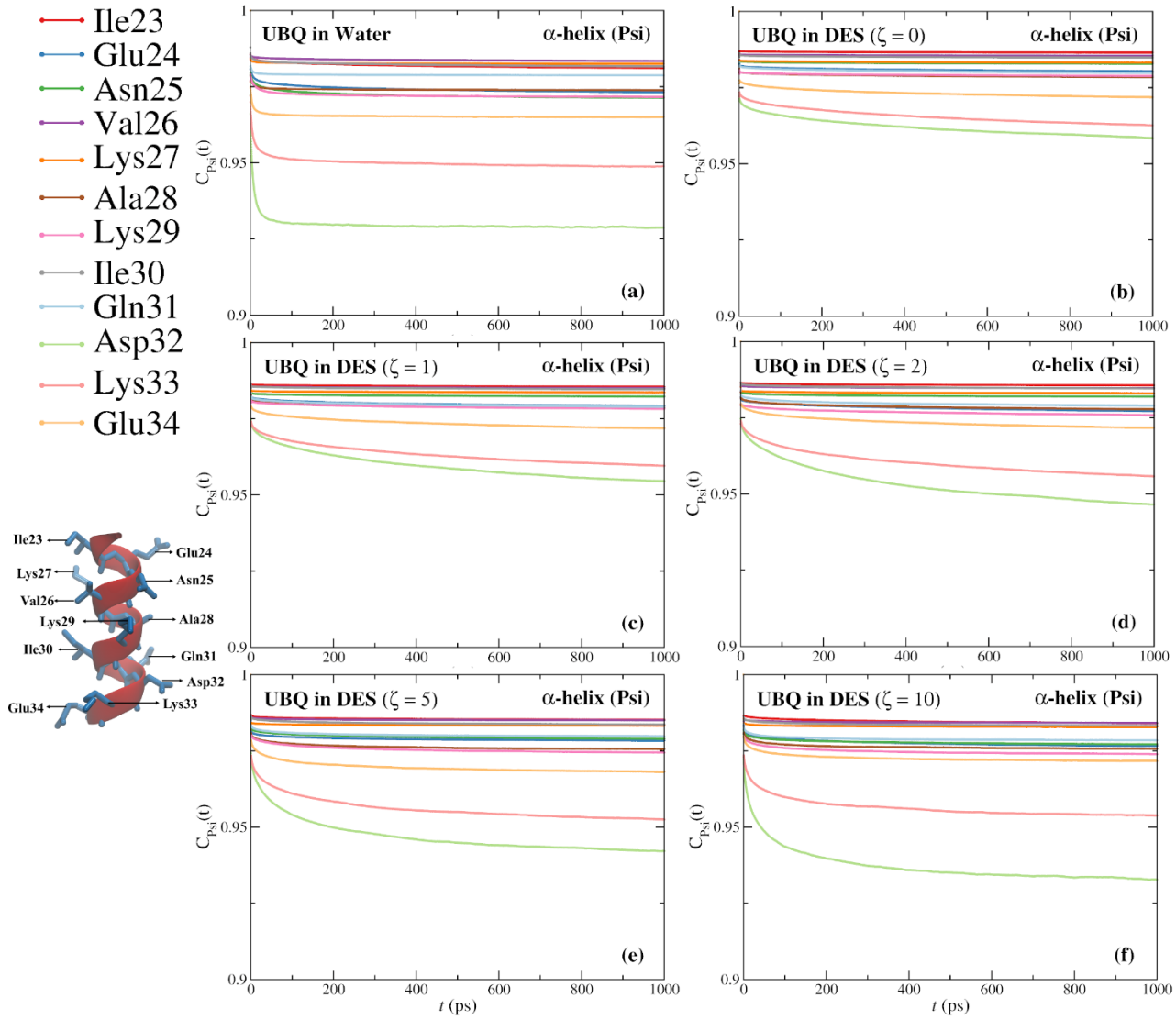

Figure 3 – Torsional dynamics time correlation functions for the α-helix (amino acids 23-34) psi angles of UBQ in water and in the DES with distinct water contents at 298 K and 0.1 MPa.

The slaving model is closely associated with the solvent's viscosity. Ansari *et al.*[75] long showed that the rate of protein conformational changes (myoglobin structural relaxation upon CO release) was approximately given by the inverse first power of the viscosity, as predicted by Kramers theory in the high friction limit[76]. However, a fractional dependence of the viscosity is also observed for some proteins and peptides, including an α-helix peptide[72,77]. We stress that the viscosity of many DES, and Bet:Gly, in particular, is much higher (~1500 mPas) than that of liquid water (~1 mPas) and the solvents (e.g., glycerol-water, glucose-water) commonly used to study the effect of the viscosity on protein folding rates[72,75,77]. A similar difference of order of magnitude characterizes the

diffusion coefficients of the model DES components (~0.001×10^{-5} cm^2s^{-1}; **Table 1**) and TIP4P-Ew water[69] (2.3×10^{-5} cm^2s^{-1}). The viscosity of the model DES for $\zeta = 5$ (26 mPas) and $\zeta = 10$ (7.3 mPas) is, however, significantly lower, and more similar to that of the solvents used in the abovementioned protein folding studies. However, the addition of water to the DES, while lowering the viscosity in a monotonic way and activating α-fluctuations, will not equally favor the dynamics of all solvent exposed protein segments (β-fluctuations), since a complete (homogeneous) hydration shell does not readily form. For instance, even within the α-helix torsions it can be seen that water addition does not impact the same way all backbone torsions. This is particularly clear for some amino acids (see **Fig.(3)**). If protein torsions are thought of as elementary kinetic steps underlying large-scale motions associated with protein folding/unfolding, this heterogeneous, non-monotonic hydration, could explain the non-monotonic behavior of R_g (see **Fig. 2a**) as well as the non-monotonic protein folding behavior recently reported for other DESs[20]. To probe this picture, we calculated the C_α-OW coordination numbers (CNs) from the respective RDFs for each amino acid in the alpha-helix. **Figure 4(a)** shows that water works as a lubricant of the torsional dynamics, unraveling the reason for Asp32, Lys33, and Glu34 to have the fastest ψ and ϕ dihedral dynamics (i.e., a higher hydration). On the other hand, the smaller slowdown factor found for Glu24 can be readily explained by the smaller difference between the C_α hydration amongst the different aqueous mixtures. Additionally, **Fig. 4(a)** shows that the backbone hydration does not vary monotonically next to every amino acid with the water content. The C_α-OW CNs in **Fig. 4** were obtained through integration of the RDF up to the respective first minimum determined for UBQ in water (see **Table S5**). Since the latter vary from amino acid to amino acid, we also calculated the CNs up to 5.5 Å for every amino acid (**see Fig. S7**). A similar trend can be observed, the main difference being a larger hydration of Lys29, which explains the relatively fast decay of the torsional time correlation function. A similar calculation was performed for the respective C and N atoms of the backbone involved in the torsional dynamics (**Fig. S7**).

In addition to the number of water molecules the water dynamics (*e.g.*, rotational dynamics) should be key to the protein motions. The dynamics of water will depend on the local environment regarding the number of water neighbors, protein volume exclusion, and protein-water and water-solvent interactions. **Figure 4(b-f)** display the orientational dynamics time correlation functions (eq. (6) with $l = 2$) for water molecules in the first hydration shell of the C_α of the same amino acids. As can be seen, while the orientational dynamics increases, in general, with the water content, this increase is not equal for all amino acids across the different solutions. The orientational dynamics of water next to Asp32, Lys33, and Glu34 is among the fastest, consistent with the torsional dynamics of UBQ. A similar correlation can be seen concerning Asn25, Ala28, Lys29, and Gln31, especially in water,

where a fast torsional dynamics and orientational dynamics of water are observed, whereas water near Ile23 is nearly immobilized. The relatively fast orientational dynamics of water next to Ile30 in water seems to contradict this picture, nonetheless. However, a closer look shows that Ile30 has less than a water molecule in the hydration shell (~ 0.8), in average, and this water molecule already appears at a long distance from the C_α (see **Table S5**), thus, possibly sharing the shell of the nearest neighbors Lys29 and Gln31 which display a faster orientational dynamics.

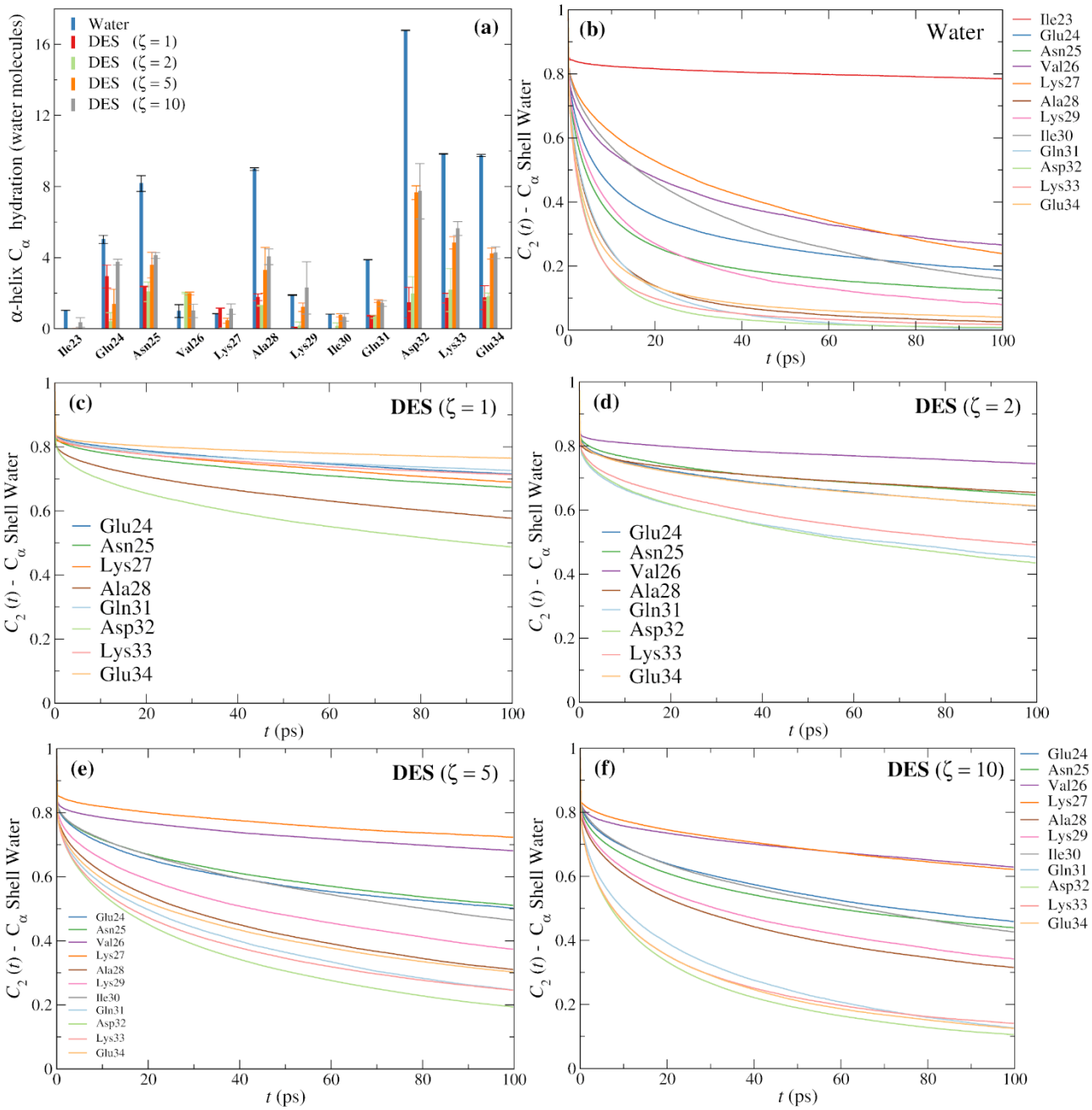

Figure 4 – (a) Water coordination of the C_α of each amino acid from UBQ's α-helix in water and in the different DES-water mixtures. **(b)** to **(f)** give the orientational time correlation function of water molecules in the first hydration shell of the C_α of each amino acid from UBQ's α-helix.

The above analysis shows that the torsional dynamics depends both on the solvent viscosity (α-

fluctuations) and protein-solvation shell coupled dynamics (β-fluctuations), in accord with the slaving mechanism[74]. However, this dependence is not monotonic for all the amino acids. **Figure 5** shows the dihedral time correlation functions of Asp32 and Glu24 and the orientational dynamics of water molecules in the respective C_α's hydration shell, for which a monotonic and non-monotonic variation of $1/\tau$ with the viscosity is observed, respectively.

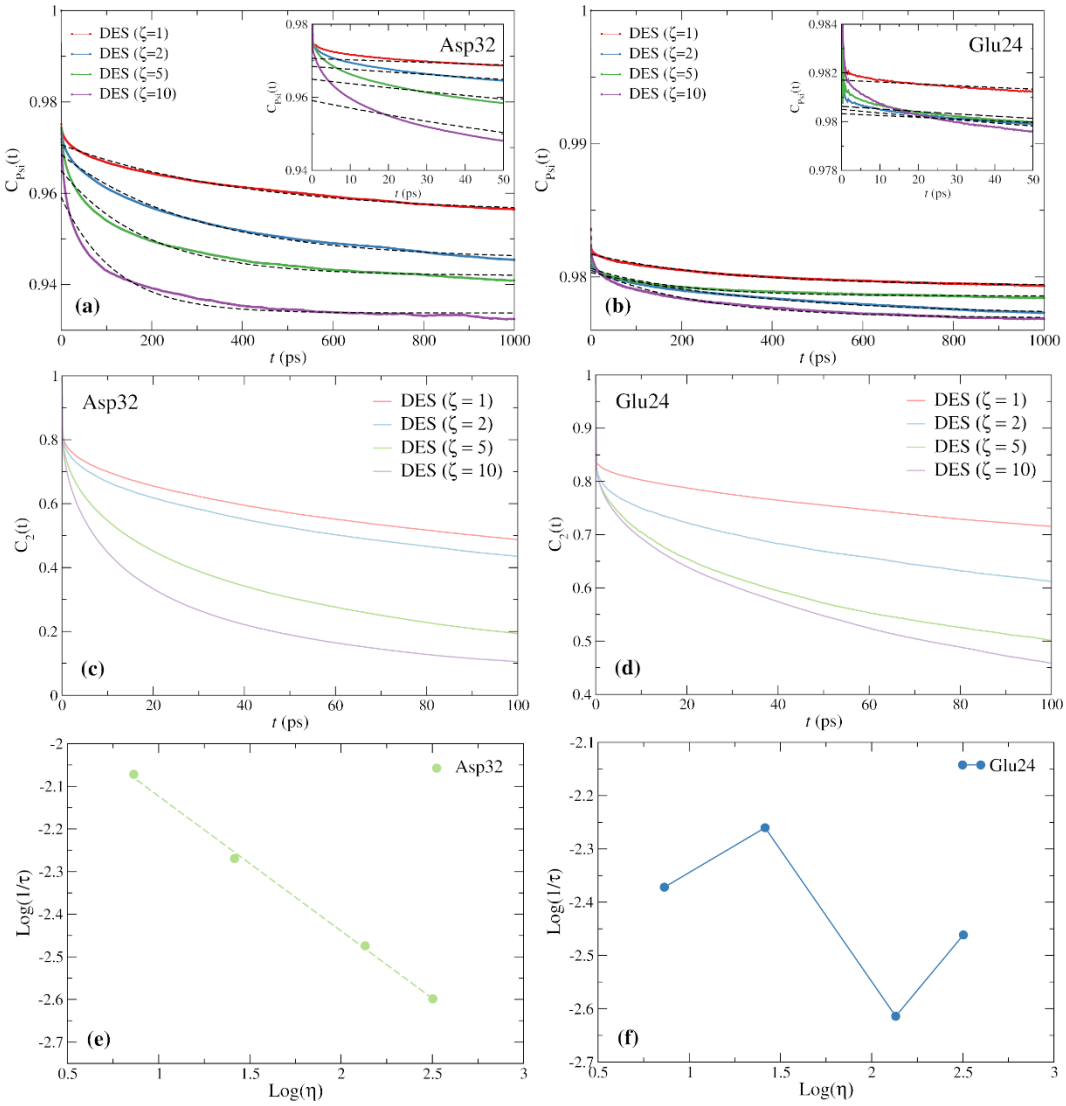

Figure 5 – Torsional dynamics of **(a)** Asp32 and **(b)** Glu24 (dashed lines are fits to eq. (8)); Orientational dynamics of water molecules in C_α hydration shell of **(c)** Asp32 and **(d)** Glu24; Logarithm of the inverse of the torsional relaxation time as a function of the viscosity for **(e)** Asp32, which exhibits a power law dependence of the viscosity, $1/\tau = A\eta^{-\gamma}$, with exponent $\gamma = 0.31$ (dashed line is a linear fit), and **(f)** Glu24, which exhibits a non-monotonic dependence of the viscosity (solid line is a guide to the eye).

Thus, whereas a fractional dependence of the viscosity (i.e., a power law dependence with an exponent of 0.31 is found for Asp32, a non-monotonic variation is found for Glu24. In spite of the limitations of eq. (8), this behavior should be connected with a non-monotonic hydration of some backbone atoms involved in the torsional dynamics of the protein (i.e., ψ and ϕ torsions). Since the conformational dynamics and, therefore, folding and unfolding, involve multiple torsions, this can

explain the non-monotonic behavior of protein folding with the water content in a DES, as observed experimentally[20]. We stress, nonetheless, that there has been experimental reports where the amount of water is inversely correlated with a protein's ability to refold[9]; the reason for this behavior is not clear.

While the results discussed above support the DES's competence to preserve the protein's structure they also indicate a major loss of conformational dynamics, which for some proteins, including enzymes, can mean a loss of function, only recovered upon water addition. Additionally, we stress that the protein protection mechanism envisaged here does not consider the protein's potential energy surface dependence of the solvent, and, therefore, putative thermodynamic perturbations of a two-state F ⇌ U equilibrium.

We now discuss the thermal stability of UBQ in water and the DES. To assess the thermal stability of the protein we first analyzed the root mean square displacement (RMSD), the percentage of α-helix and β-sheet, as well as the R_g and the solvent accessible surface area (SASA) of UBQ in water and in the DES at temperatures ranging from 373 K to 450 K; the reason for such a high maximum temperature was the fact that the protein did not unfold in the DES below 450 K within 2 μs.

Figure 6 shows the RMSD of UBQ in water and in the DES for two replicas. The second replica (R_2) in water was performed with a time-step of 1 fs. While the protein is more stable at the lowest temperatures in R_2, a similar stability enhancement is not observed at 425 K and 450 K, ruling out any strong time-step dependence. A similar behavior was found for R_g and SASA (see **Figs S8** and **S9**). The effect of pressure on the water systems was also ruled out, with UBQ in water at high temperatures and 0.1 MPa, and UBQ in the DES at the same pressures used to simulate the protein in water, showing similar results to those displayed in **Fig. 6 (see Fig. S10)**.

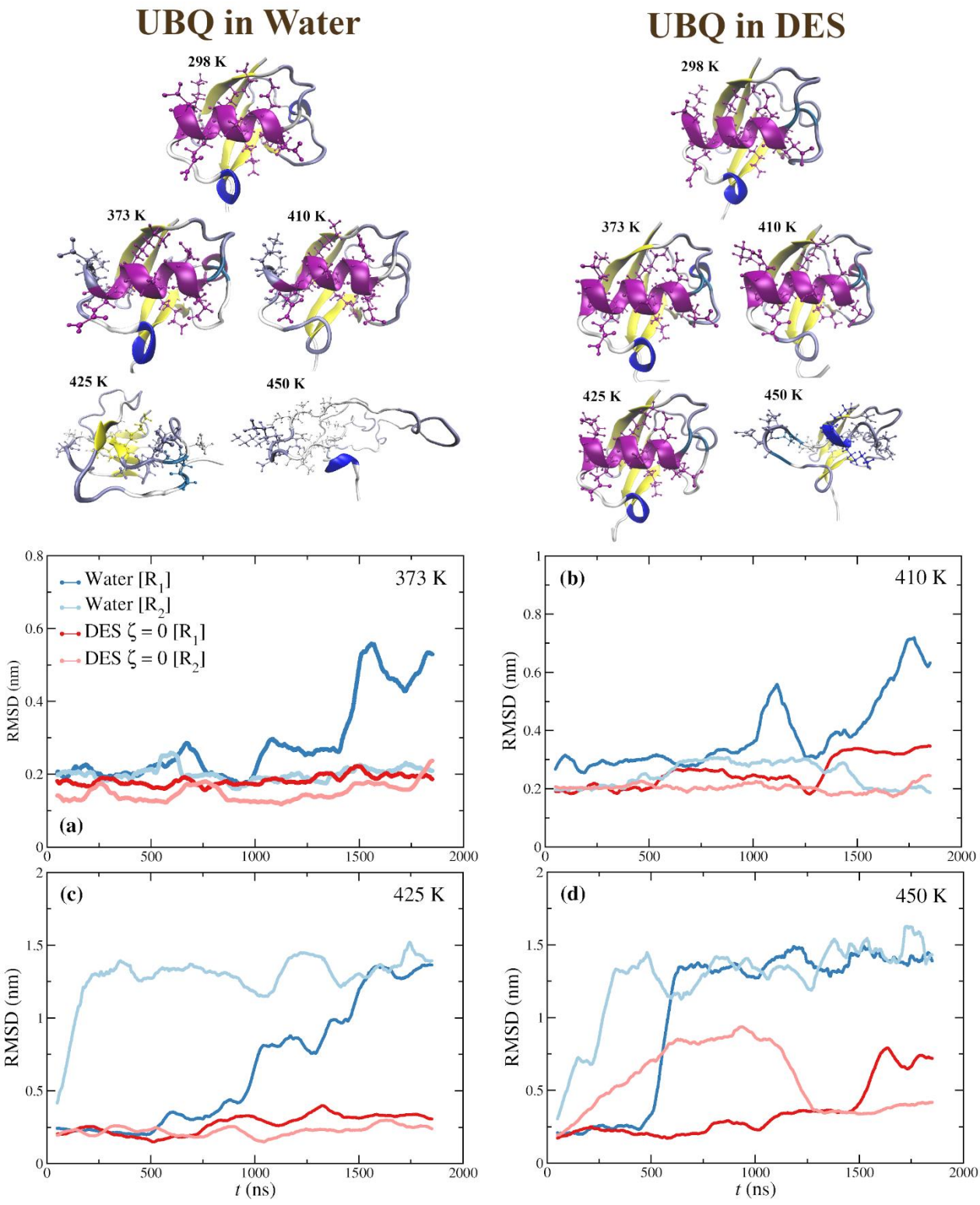

Figure 6 – Upper panel: Last conformation of UBQ in water (R_2) and in the DES (R_2) from 1.9 μs trajectories at different temperatures. Lower panel: RMSD of UBQ (backbone), relative to the crystal structure, along the trajectories in water and in the DES at four temperatures. The data are moving averages computed with a window of 100 ns. Notice the different RMSD scales between (a), (b) and (c-d).

Figure 6 (upper panel) suggests that, within the timeframe of the simulations, the protein starts to melt (in water) at 373 K with the partial unfolding of the α-helix; the melting temperature of UBQ is predicted to be around 370 K[78]. **Figure 7** is consistent with this picture showing that fluctuations of

the α-helix in water start at 373 K although these are reversible. Lower fluctuations are found in the DES, increasing significantly at high temperatures, making difficult to conclude on the thermal stability differences in the solvents. β-sheet fluctuations are less ambiguous, and a higher preservation can be seen in the DES at every temperature.

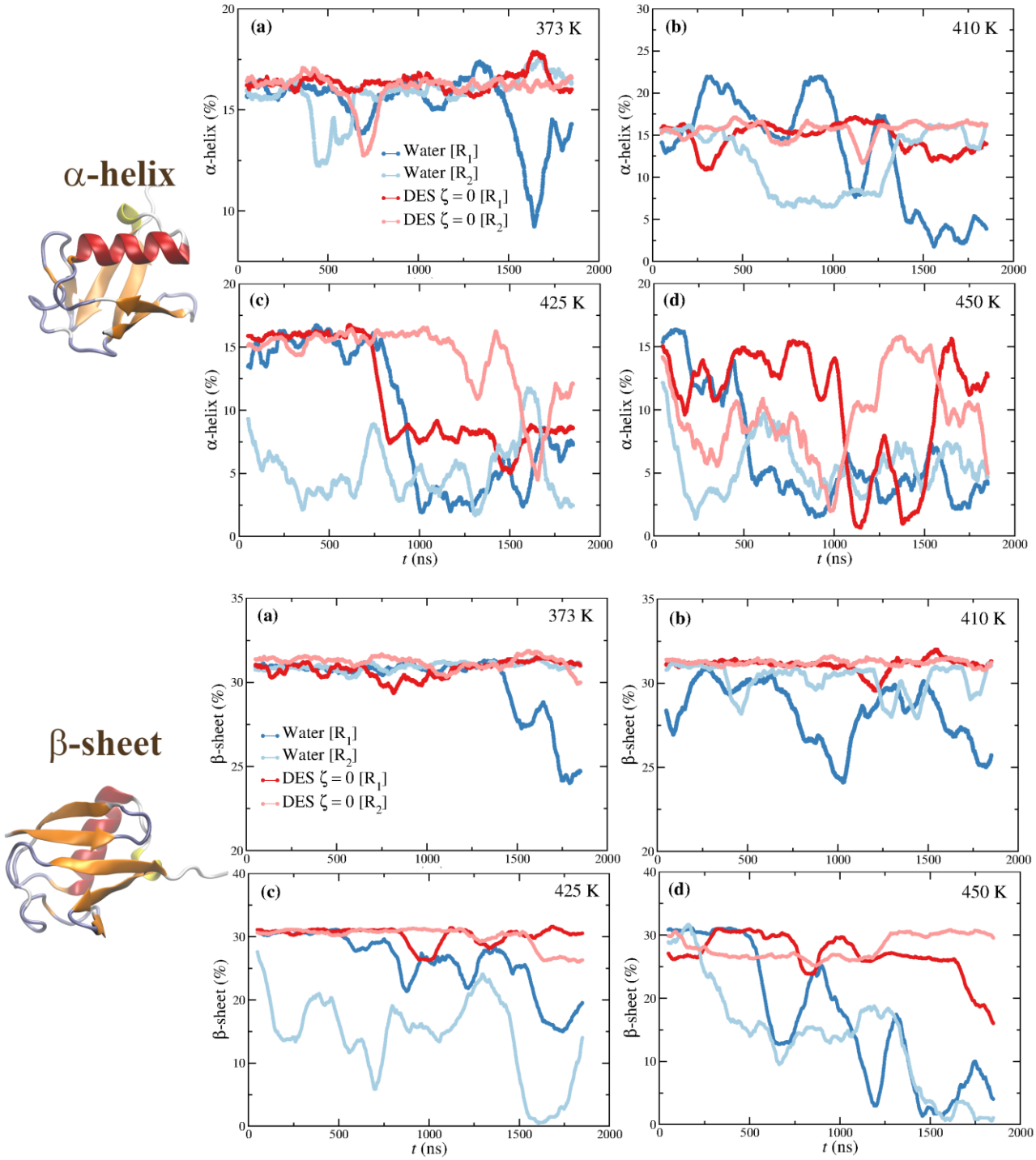

Figure 7 – Upper panel: α-helix (%) of UBQ along the trajectories in water and in the DES at four temperatures. Lower panel: β-sheet (%) of UBQ along the trajectories in water and in the DES at four temperatures. The data are moving averages computed with a window of 100 ns.

We also analyzed the dihedral time-correlation functions of the α-helix at the different

temperatures. Again, since the angles ϕ and ψ largely determine the secondary structure of a protein, these are, therefore, a good probe of the thermal stability of the protein. **Figure 8** demonstrates that these angles are highly conserved in the DES even at high temperatures, despite the less obvious differences between the percentage of α-helix denoted in **Fig. 7**. The protein is much more labile in water, concerning torsions around the C_α-C bond (ψ angle), and N-C_α (ϕ angle), whereas the DES "freezes" these rotations up to very high temperatures.

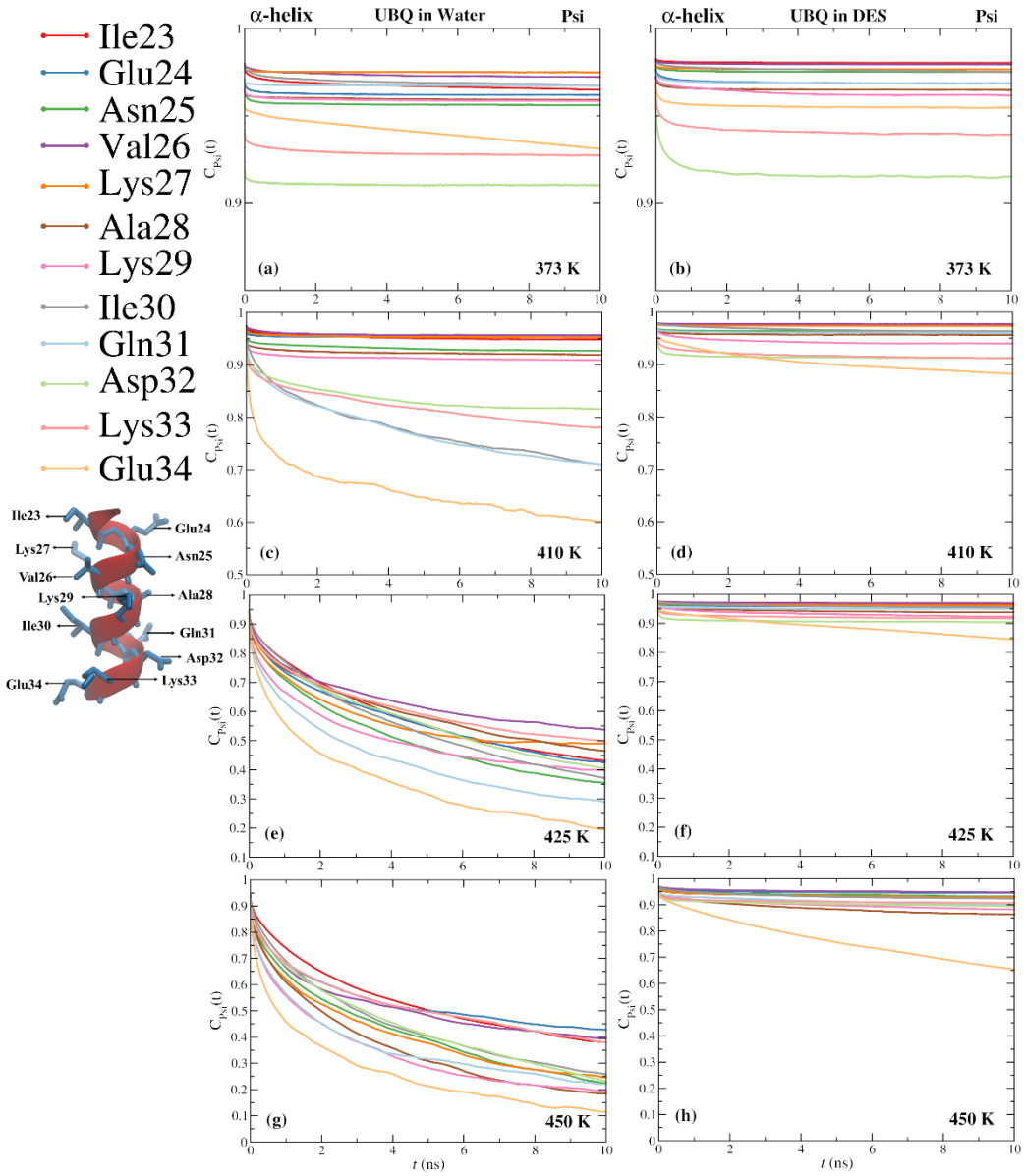

Figure 8 – Torsional dynamics time correlation functions for the α-helix (amino acids 22-34) psi angles of UBQ in water and in the DES at the different temperatures. Notice the different scales in the *y*-axis used across the different systems (for clarity).

The viscosity of the DES at these high temperatures was found to be much lower than that of the DES at 298 K and ζ = 1 and 2. Thus, η = 21±0.3 mPa·s, η = 8±0.3 mPa·s, η = 6±0.2 mPa·s, and η =

4±0.1 mPa·s at 373 K , 410 K, 425 K, and 450 K, respectively. The viscosity at 298 K and $\zeta = 5$ is 26±0.5 mPa·s and $\zeta = 10$ is 7±0.2 mPa·s, whereas at $\zeta = 1$ and $\zeta = 2$ is, respectively, 318±5 mPa·s and 135±2 mPa·s. Nevertheless, when we compare the torsional dynamics at high temperatures (425 K and 450 K) and high water molar ratios ($\zeta = 5$, 10) the former is only slightly faster (see **Fig. S11**), highlighting the importance of water to the dynamics of the protein.

A similar conclusion regarding the protein's structural fluctuations was found for the phi torsion angles, although a slower dynamics, reflected in a slower decay of the dihedral time correlation functions was observed (see **Fig. S12**). These results indicate that the slow rotational and translational dynamics of the DES's components (i.e., Bet and Gly), compared to water, along with steric hindrance and strong protein-solvent electrostatic interactions, stabilize UBQ's secondary structure by slowing down the protein conformational dynamics. Thus, protein conformational fluctuations become sequestrated by the solvent's slow dynamics, resulting in long dihedral relaxation times, and, therefore, persistent protein intramolecular hydrogen-bonds, responsible for the protein's secondary structure. From a "protein slaved" model viewpoint (in spite of the absence of water) this means that unfolding proceeds with an unfolding rate coefficient k_u much smaller than the solvent's fluctuations, and, therefore, our results indicate that UBQ can be preserved in the DES for longer times and higher temperatures than in water.

IV. Conclusions

Deep eutectic solvents (DESs) emerged as potential alternative solvent media in areas such as biocatalysis and biomolecular (cryo)preservation due to their physicochemical properties, low toxicity, ease of preparation, and reduced cost, compared to some room temperature ionic liquids and common organic solvents. From a fundamental and practical viewpoint understanding DESs' biomolecular protection mechanisms and their similarities with intracellular protective osmolytes, synthesized by some living organisms to cope with adverse environmental conditions, is of great interest. Herein, we studied the structure of a small protein (ubiquitin) in water and a B:G:W DES at varying water molar ratios and temperatures ranging from 298 K to 450 K. Our results show that even at large molar fractions of water, betaine, and glycerol, are not excluded from the protein's interface, opposite to a preferential exclusion/preferential hydration or ("biological") water entrapment mechanism. This mechanism provides a thermodynamic explanation for the stability of proteins in osmolytes' solutions. On the other hand, the slaving mechanism seeks a kinetic explanation to the viscosity and temperature dependence of the folding/unfolding rates in different environments. Our results cannot be explained by the former mechanism. However, a clear impact on the torsional dynamics of the protein is observed, which can be thought of as elementary kinetic steps underlying

large-scale motions associated with protein folding/unfolding. Thus, the DES induces an exceedingly slow conformational dynamics, compared to water, resulting in the preservation of the secondary structure of the protein. This can, therefore, be explained within the framework of protein slaving. In particular, our results highlight the importance of protein-solvent shell coupled fluctuations (β-fluctuations) manifested in a non-monotonic dependence of the torsional dynamics on the viscosity. Thus, our results show that the torsional dynamics closely depends on the viscosity (bulk) and on the protein solvent shell (local), in particular, the number of water molecules that penetrate the solvation shell and their dynamics. In this sense, such a kinetic mechanism is opposite to a preferential hydration mechanism, since suppression of fluctuations is inversely related with the number of water molecules around the protein. These results can explain a recent report where protein folding in some DES was shown to be non-monotonic with the water molar ratio.

Additionally, our results show that the protein dissolved in the DES only unfolds at very high temperatures for similar reasons. Thus, in spite of a much lower viscosity and high thermal energy, the protein's dynamics remains largely frozen due to a rigid solvation shell in the absence of water molecules.

Acknowledgements

NG acknowledges financial support from Fundação para a Ciência e a Tecnologia (FCT) of Portugal (CEECIND/00821/2017). IG and NG acknowledge support from UIDB/04046/2020 and UIDP/04046/2020 centre grants from FCT, Portugal (to BioISI) and the Portuguese National Distributed Computing Infrastructure (http://www.incd.pt).

Supporting Information

The Supporting Information is available free of charge.

Table S1 - GAFF/RESP force field parameters for betaine.
Table S2 - GAFF/RESP force field parameters for glycerol.
Table S3 - Density and viscosity of the Bet:Gly DES as a function of λ_Q.
Table S4 - Density and viscosity of the Bet:Gly DES as a function of λ_σ.
Table S5 - UBQ α-helix C_α-OW RDF minima in neat water and respective coordination.
Figure S1 - Molecular representation of betaine and glycerol.
Figure S2 - Density and viscosity of the Bet:Gly DES as a function of λ_Q and λ_σ.
Figure S3 - Bet-Bet, Bet-Gly, and Gly-Gly RDFs for the B:G (1:2) DES.
Figure S4 - Bet-Bet, Bet-Gly, Gly-Gly, Bet-OW, Gly-OW, and OW-OW RDFs for (B:G:W) (1:2:ζ; ζ = 0, 1, 2, 5, and 10).
Figure S5 –Torsional time correlation functions for the α-helix of UBQ (phi) in water and the DES for different ζ.
Figure S6 – Torsional dynamics time correlation functions for the amino acids Asp32 and Glu34 in water and the DES at different water fractions.
Figure S7 - Water coordination of the backbone C_α, C, and N for each amino acid of UBQ's α-helix.
Figure S8 - Radius of gyration of UBQ along the trajectories in water and in the DES at four temperatures
Figure S9 - Solvent-accessible surface area of UBQ along the trajectories in water and in the DES at four

temperatures.
Figure S10 – UBQ RMSD for replica 3 (R_3) in water and DES – pressure effect.
Figure S11 – Torsional dynamics in aqueous DES (ζ = 5, 10) at 298 K and anhydrous (ζ = 0) DES at high temperatures (425 K and 450 K).
Figure S12 -Torsional dynamics time correlation functions for the α-helix of UBQ (phi) in water and the DES at different temperatures.

References

(1) Hansen, B. B.; Spittle, S.; Chen, B.; Poe, D.; Zhang, Y.; Klein, J. M.; Horton, A.; Adhikari, L.; Zelovich, T.; Doherty, B. W.; Gurkan, B.; Maginn, E. J.; Ragauskas, A.; Dadmun, M.; Zawodzinski, T. A.; Baker, G. A.; Tuckerman, M. E.; Savinell, R. F.; Sangoro, J. R. Deep Eutectic Solvents: A Review of Fundamentals and Applications. *Chem. Rev.* **2021**, *121* (3), 1232–1285. https://doi.org/10.1021/acs.chemrev.0c00385.

(2) Smith, E. L.; Abbott, A. P.; Ryder, K. S. Deep Eutectic Solvents (DESs) and Their Applications. *Chem. Rev.* **2014**, *114* (21), 11060–11082. https://doi.org/10.1021/cr300162p.

(3) Abbott, A. P.; Capper, G.; Davies, D. L.; Rasheed, R. K.; Tambyrajah, V. Novel Solvent Properties of Choline Chloride/Urea MixturesElectronic Supplementary Information (ESI) Available: Spectroscopic Data. See Http://Www.Rsc.Org/Suppdata/Cc/B2/B210714g/. *Chem. Commun.* **2003**, No. 1, 70–71. https://doi.org/10.1039/b210714g.

(4) Paiva, A.; Craveiro, R.; Aroso, I.; Martins, M.; Reis, R. L.; Duarte, A. R. C. Natural Deep Eutectic Solvents – Solvents for the 21st Century. *ACS Sustain. Chem. Eng.* **2014**, *2* (5), 1063–1071. https://doi.org/10.1021/sc500096j.

(5) Gorke, J. T.; Srienc, F.; Kazlauskas, R. J. Hydrolase-Catalyzed Biotransformations in Deep Eutectic Solvents. *Chem. Commun.* **2008**, No. 10, 1235. https://doi.org/10.1039/b716317g.

(6) Esquembre, R.; Sanz, J. M.; Wall, J. G.; del Monte, F.; Mateo, C. R.; Ferrer, M. L. Thermal Unfolding and Refolding of Lysozyme in Deep Eutectic Solvents and Their Aqueous Dilutions. *Phys. Chem. Chem. Phys.* **2013**, *15* (27), 11248. https://doi.org/10.1039/c3cp44299c.

(7) Kumar, N.; Kishore, N. Protein Stabilization and Counteraction of Denaturing Effect of Urea by Glycine Betaine. *Biophys. Chem.* **2014**, *189*, 16–24. https://doi.org/10.1016/j.bpc.2014.03.001.

(8) Monhemi, H.; Housaindokht, M. R.; Moosavi-Movahedi, A. A.; Bozorgmehr, M. R. How a Protein Can Remain Stable in a Solvent with High Content of Urea: Insights from Molecular Dynamics Simulation of Candida Antarctica Lipase B in Urea : Choline Chloride Deep Eutectic Solvent. *Phys. Chem. Chem. Phys.* **2014**, *16* (28), 14882. https://doi.org/10.1039/c4cp00503a.

(9) Sun, H.; Xin, R.; Qu, D.; Yao, F. Mechanism of Deep Eutectic Solvents Enhancing Catalytic Function of Cytochrome P450 Enzymes in Biosynthesis and Organic Synthesis. *J. Biotechnol.* **2020**, *323*, 264–273. https://doi.org/10.1016/j.jbiotec.2020.07.004.

(10) Durand, E.; Lecomte, J.; Villeneuve, P. Deep Eutectic Solvents: Synthesis, Application, and Focus on Lipase-catalyzed Reactions. *Eur. J. Lipid Sci. Technol.* **2013**, *115* (4), 379–385. https://doi.org/10.1002/ejlt.201200416.

(11) Pätzold, M.; Siebenhaller, S.; Kara, S.; Liese, A.; Syldatk, C.; Holtmann, D. Deep Eutectic Solvents as Efficient Solvents in Biocatalysis. *Trends Biotechnol.* **2019**, *37* (9), 943–959. https://doi.org/10.1016/j.tibtech.2019.03.007.

(12) Kist, J. A.; Henzl, M. T.; Bañuelos, J. L.; Baker, G. A. Calorimetric Evaluation of the Operational Thermal Stability of Ribonuclease A in Hydrated Deep Eutectic Solvents. *ACS Sustain. Chem. Eng.* **2019**, *7* (15), 12682–12687. https://doi.org/10.1021/acssuschemeng.9b02585.

(13) Kist, J. A.; Zhao, H.; Mitchell-Koch, K. R.; Baker, G. A. The Study and Application of

Biomolecules in Deep Eutectic Solvents. *J. Mater. Chem. B* **2021**, *9* (3), 536–566. https://doi.org/10.1039/D0TB01656J.
(14) Gajardo-Parra, N. F.; Meneses, L.; Duarte, A. R. C.; Paiva, A.; Held, C. Assessing the Influence of Betaine-Based Natural Deep Eutectic Systems on Horseradish Peroxidase. *ACS Sustain. Chem. Eng.* **2022**, *10* (38), 12873–12881. https://doi.org/10.1021/acssuschemeng.2c04045.
(15) Kim, S. H.; Park, S.; Yu, H.; Kim, J. H.; Kim, H. J.; Yang, Y.-H.; Kim, Y. H.; Kim, K. J.; Kan, E.; Lee, S. H. Effect of Deep Eutectic Solvent Mixtures on Lipase Activity and Stability. *J. Mol. Catal. B Enzym.* **2016**, *128*, 65–72. https://doi.org/10.1016/j.molcatb.2016.03.012.
(16) Zeng, C.-X.; Qi, S.-J.; Xin, R.-P.; Yang, B.; Wang, Y.-H. Enzymatic Selective Synthesis of 1,3-DAG Based on Deep Eutectic Solvent Acting as Substrate and Solvent. *Bioprocess Biosyst. Eng.* **2015**, *38* (11), 2053–2061. https://doi.org/10.1007/s00449-015-1445-0.
(17) Juneidi, I.; Hayyan, M.; Hashim, M. A.; Hayyan, A. Pure and Aqueous Deep Eutectic Solvents for a Lipase-Catalysed Hydrolysis Reaction. *Biochem. Eng. J.* **2017**, *117*, 129–138. https://doi.org/10.1016/j.bej.2016.10.003.
(18) Sanchez-Fernandez, A.; Prevost, S.; Wahlgren, M. Deep Eutectic Solvents for the Preservation of Concentrated Proteins: The Case of Lysozyme in 1 : 2 Choline Chloride : Glycerol. *Green Chem.* **2022**, *24* (11), 4437–4442. https://doi.org/10.1039/D1GC04378A.
(19) Sanchez-Fernandez, A.; Edler, K. J.; Arnold, T.; Alba Venero, D.; Jackson, A. J. Protein Conformation in Pure and Hydrated Deep Eutectic Solvents. *Phys. Chem. Chem. Phys.* **2017**, *19* (13), 8667–8670. https://doi.org/10.1039/C7CP00459A.
(20) Sanchez-Fernandez, A.; Basic, M.; Xiang, J.; Prevost, S.; Jackson, A. J.; Dicko, C. Hydration in Deep Eutectic Solvents Induces Non-Monotonic Changes in the Conformation and Stability of Proteins. *J. Am. Chem. Soc.* **2022**, *144* (51), 23657–23667. https://doi.org/10.1021/jacs.2c11190.
(21) Cao, J.; Wu, R.; Zhu, F.; Dong, Q.; Su, E. Enzymes in Nearly Anhydrous Deep Eutectic Solvents: Insight into the Biocompatibility and Thermal Stability. *Enzyme Microb. Technol.* **2022**, *157*, 110022. https://doi.org/10.1016/j.enzmictec.2022.110022.
(22) Sanchez-Fernandez, A.; Jackson, A. J. Proteins in Deep Eutectic Solvents: Structure, Dynamics and Interactions with the Solvent. In *Advances in Botanical Research*; Elsevier, 2021; Vol. 97, pp 69–94. https://doi.org/10.1016/bs.abr.2020.09.003.
(23) Khodaverdian, S.; Dabirmanesh, B.; Heydari, A.; Dashtban-moghadam, E.; Khajeh, K.; Ghazi, F. Activity, Stability and Structure of Laccase in Betaine Based Natural Deep Eutectic Solvents. *Int. J. Biol. Macromol.* **2018**, *107*, 2574–2579. https://doi.org/10.1016/j.ijbiomac.2017.10.144.
(24) Yadav, N.; Bhakuni, K.; Bisht, M.; Bahadur, I.; Venkatesu, P. Expanding the Potential Role of Deep Eutectic Solvents toward Facilitating the Structural and Thermal Stability of α-Chymotrypsin. *ACS Sustain. Chem. Eng.* **2020**, *8* (27), 10151–10160. https://doi.org/10.1021/acssuschemeng.0c02213.
(25) Hossain, S. S.; Paul, S.; Samanta, A. Structural Stability and Conformational Dynamics of Cytochrome c in Hydrated Deep Eutectic Solvents. *J. Phys. Chem. B* **2021**, *125* (22), 5757–5765. https://doi.org/10.1021/acs.jpcb.1c01975.
(26) Toledo, M. L.; Pereira, M. M.; Freire, M. G.; Silva, J. P. A.; Coutinho, J. A. P.; Tavares, A. P. M. Laccase Activation in Deep Eutectic Solvents. *ACS Sustain. Chem. Eng.* **2019**, *7* (13), 11806–11814. https://doi.org/10.1021/acssuschemeng.9b02179.
(27) De Gonzalo, G.; Martin, C.; Fraaije, M. W. Positive Impact of Natural Deep Eutectic Solvents on the Biocatalytic Performance of 5-Hydroxymethyl-Furfural Oxidase. *Catalysts* **2020**, *10* (4), 447. https://doi.org/10.3390/catal10040447.
(28) Hümmer, M.; Kara, S.; Liese, A.; Huth, I.; Schrader, J.; Holtmann, D. Synthesis of (-)-Menthol Fatty Acid Esters in and from (-)-Menthol and Fatty Acids – Novel Concept for Lipase Catalyzed Esterification Based on Eutectic Solvents. *Mol. Catal.* **2018**, *458*, 67–72. https://doi.org/10.1016/j.mcat.2018.08.003.

(29) Weng, L.; Stott, S. L.; Toner, M. Exploring Dynamics and Structure of Biomolecules, Cryoprotectants, and Water Using Molecular Dynamics Simulations: Implications for Biostabilization and Biopreservation. *Annu. Rev. Biomed. Eng.* **2019**, *21* (1), 1–31. https://doi.org/10.1146/annurev-bioeng-060418-052130.
(30) Jesus, A. R.; Duarte, A. R. C.; Paiva, A. Use of Natural Deep Eutectic Systems as New Cryoprotectant Agents in the Vitrification of Mammalian Cells. *Sci. Rep.* **2022**, *12* (1), 8095. https://doi.org/10.1038/s41598-022-12365-4.
(31) Bryant, S. J.; Awad, M. N.; Elbourne, A.; Christofferson, A. J.; Martin, A. V.; Meftahi, N.; Drummond, C. J.; Greaves, T. L.; Bryant, G. Deep Eutectic Solvents as Cryoprotective Agents for Mammalian Cells. *J. Mater. Chem. B* **2022**, *10* (24), 4546–4560. https://doi.org/10.1039/D2TB00573E.
(32) Gertrudes, A.; Craveiro, R.; Eltayari, Z.; Reis, R. L.; Paiva, A.; Duarte, A. R. C. How Do Animals Survive Extreme Temperature Amplitudes? The Role of Natural Deep Eutectic Solvents. *ACS Sustain. Chem. Eng.* **2017**, *5* (11), 9542–9553. https://doi.org/10.1021/acssuschemeng.7b01707.
(33) Hua, L.; Zhou, R.; Thirumalai, D.; Berne, B. J. Urea Denaturation by Stronger Dispersion Interactions with Proteins than Water Implies a 2-Stage Unfolding. *Proc. Natl. Acad. Sci.* **2008**, *105* (44), 16928–16933. https://doi.org/10.1073/pnas.0808427105.
(34) Xavier, P.; Galamba, N. Effect of Urea on the Hydration and Aggregation of Hydrophobic and Amphiphilic Solute Models: Implications to Protein Aggregation. *J. Chem. Phys.* **2021**, *155* (14), 144501. https://doi.org/10.1063/5.0064707.
(35) Choi, Y. H.; Van Spronsen, J.; Dai, Y.; Verberne, M.; Hollmann, F.; Arends, I. W. C. E.; Witkamp, G.-J.; Verpoorte, R. Are Natural Deep Eutectic Solvents the Missing Link in Understanding Cellular Metabolism and Physiology? *Plant Physiol.* **2011**, *156* (4), 1701–1705. https://doi.org/10.1104/pp.111.178426.
(36) Asakura, S.; Oosawa, F. On Interaction between Two Bodies Immersed in a Solution of Macromolecules. *J. Chem. Phys.* **1954**, *22* (7), 1255–1256. https://doi.org/10.1063/1.1740347.
(37) Yancey, P. H.; Clark, M. E.; Hand, S. C.; Bowlus, R. D.; Somero, G. N. Living with Water Stress: Evolution of Osmolyte Systems. *Science* **1982**, *217* (4566), 1214–1222. https://doi.org/10.1126/science.7112124.
(38) Lee, J. C.; Timasheff, S. N. The Stabilization of Proteins by Sucrose. *J. Biol. Chem.* **1981**, *256* (14), 7193–7201. https://doi.org/10.1016/S0021-9258(19)68947-7.
(39) Arakawa, T.; Timasheff, S. N. The Stabilization of Proteins by Osmolytes. *Biophys. J.* **1985**, *47* (3), 411–414. https://doi.org/10.1016/S0006-3495(85)83932-1.
(40) Cheung, M. S.; Klimov, D.; Thirumalai, D. Molecular Crowding Enhances Native State Stability and Refolding Rates of Globular Proteins. *Proc. Natl. Acad. Sci.* **2005**, *102* (13), 4753–4758. https://doi.org/10.1073/pnas.0409630102.
(41) Xie, G.; Timasheff, S. N. The Thermodynamic Mechanism of Protein Stabilization by Trehalose. *Biophys. Chem.* **1997**, *64* (1–3), 25–43. https://doi.org/10.1016/S0301-4622(96)02222-3.
(42) Street, T. O.; Bolen, D. W.; Rose, G. D. A Molecular Mechanism for Osmolyte-Induced Protein Stability. *Proc. Natl. Acad. Sci.* **2006**, *103* (38), 13997–14002. https://doi.org/10.1073/pnas.0606236103.
(43) Vijay-kumar, S.; Bugg, C. E.; Cook, W. J. Structure of Ubiquitin Refined at 1.8 Å Resolution. *J. Mol. Biol.* **1987**, *194* (3), 531–544. https://doi.org/10.1016/0022-2836(87)90679-6.
(44) Vijay-kumar, S.; Bugg, C. E.; Cook, W. J. Structure of Ubiquitin Refined at 1.8 Å Resolution. *J. Mol. Biol.* **1987**, *194* (3), 531–544. https://doi.org/10.1016/0022-2836(87)90679-6.
(45) Hornak, V.; Abel, R.; Okur, A.; Strockbine, B.; Roitberg, A.; Simmerling, C. Comparison of Multiple Amber Force Fields and Development of Improved Protein Backbone Parameters. *Proteins Struct. Funct. Bioinforma.* **2006**, *65* (3), 712–725. https://doi.org/10.1002/prot.21123.
(46) Horn, H. W.; Swope, W. C.; Pitera, J. W.; Madura, J. D.; Dick, T. J.; Hura, G. L.; Head-Gordon, T. Development of an Improved Four-Site Water Model for Biomolecular

Simulations: TIP4P-Ew. *J. Chem. Phys.* **2004**, *120* (20), 9665–9678. https://doi.org/10.1063/1.1683075.
(47) Wang, J.; Wolf, R. M.; Caldwell, J. W.; Kollman, P. A.; Case, D. A. Development and Testing of a General Amber Force Field. *J. Comput. Chem.* **2004**, *25* (9), 1157–1174. https://doi.org/10.1002/jcc.20035.
(48) Becke, A. D. Density-functional Thermochemistry. III. The Role of Exact Exchange. *J. Chem. Phys.* **1993**, *98* (7), 5648–5652. https://doi.org/10.1063/1.464913.
(49) Cornell, W. D.; Cieplak, P.; Bayly, C. I.; Kollman, P. A. Application of RESP Charges to Calculate Conformational Energies, Hydrogen Bond Energies, and Free Energies of Solvation. *J. Am. Chem. Soc.* **1993**, *115* (21), 9620–9631. https://doi.org/10.1021/ja00074a030.
(50) M. J. Frisch, G. W. Trucks, H. B. Schlegel, G. E. Scuseria, M. A. Robb, J. R. Cheeseman, G. Scalmani, V. Barone, G. A. Petersson, H. Nakatsuji, X. Li, M. Caricato, A. Marenich, J. Bloino, B. G. Janesko, R. Gomperts, B. Mennucci, H. P. Hratchian, J. V. Ortiz, A. F. Izmaylov, J. L. Sonnenberg, D. Williams-Young, F. Ding, F. Lipparini, F. Egidi, J. Goings, B. Peng, A. Petrone, T. Henderson, D. Ranasinghe, V. G. Zakrzewski, J. Gao, N. Rega, G. Zheng, W. Liang, M. Hada, M. Ehara, K. Toyota, R. Fukuda, J. Hasegawa, M. Ishida, T. Nakajima, Y. Honda, O. Kitao, H. Nakai, T. Vreven, K. Throssell, J. A. Montgomery, Jr., J. E. Peralta, F. Ogliaro, M. Bearpark, J. J. Heyd, E. Brothers, K. N. Kudin, V. N. Staroverov, T. Keith, R. Kobayashi, J. Normand, K. Raghavachari, A. Rendell, J. C. Burant, S. S. Iyengar, J. Tomasi, M. Cossi, J. M. Millam, M. Klene, C. Adamo, R. Cammi, J. W. Ochterski, R. L. Martin, K. Morokuma, O. Farkas, J. B. Foresman, and D. J. Fox,. *Gaussian 09. Revision D.01*; Gaussian, Inc.: Wallingford CT, 2016.
(51) Monteiro, H.; Paiva, A.; Duarte, A. R. C.; Galamba, N. Structure and Dynamic Properties of a Glycerol–Betaine Deep Eutectic Solvent: When Does a DES Become an Aqueous Solution? *ACS Sustain. Chem. Eng.* **2022**, *10* (11), 3501–3512. https://doi.org/10.1021/acssuschemeng.1c07461.
(52) Van Der Spoel, D.; Lindahl, E.; Hess, B.; Groenhof, G.; Mark, A. E.; Berendsen, H. J. C. GROMACS: Fast, Flexible, and Free. *J. Comput. Chem.* **2005**, *26* (16), 1701–1718. https://doi.org/10.1002/jcc.20291.
(53) Bussi, G.; Donadio, D.; Parrinello, M. Canonical Sampling through Velocity Rescaling. *J. Chem. Phys.* **2007**, *126* (1), 014101. https://doi.org/10.1063/1.2408420.
(54) Parrinello, M.; Rahman, A. Polymorphic Transitions in Single Crystals: A New Molecular Dynamics Method. *J. Appl. Phys.* **1981**, *52* (12), 7182–7190. https://doi.org/10.1063/1.328693.
(55) Essmann, U.; Perera, L.; Berkowitz, M. L.; Darden, T.; Lee, H.; Pedersen, L. G. A Smooth Particle Mesh Ewald Method. *J. Chem. Phys.* **1995**, *103* (19), 8577–8593. https://doi.org/10.1063/1.470117.
(56) Hess, B.; Bekker, H.; Berendsen, H. J. C.; Fraaije, J. G. E. M. LINCS: A Linear Constraint Solver for Molecular Simulations. *J. Comput. Chem.* **1997**, *18* (12), 1463–1472. https://doi.org/10.1002/(SICI)1096-987X(199709)18:12<1463::AID-JCC4>3.0.CO;2-H.
(57) Gross, M.; Jaenicke, R. Proteins under Pressure. The Influence of High Hydrostatic Pressure on Structure, Function and Assembly of Proteins and Protein Complexes. *Eur. J. Biochem.* **1994**, *221* (2), 617–630. https://doi.org/10.1111/j.1432-1033.1994.tb18774.x.
(58) Herberhold, H.; Winter, R. Temperature- and Pressure-Induced Unfolding and Refolding of Ubiquitin: A Static and Kinetic Fourier Transform Infrared Spectroscopy Study. *Biochemistry* **2002**, *41* (7), 2396–2401. https://doi.org/10.1021/bi012023b.
(59) Haile, J. M. *Molecular Dynamics Simulation: Elementary Methods*; Wiley professional paperback series; Wiley: New York, 1997.
(60) Daivis, P. J.; Evans, D. J. Comparison of Constant Pressure and Constant Volume Nonequilibrium Simulations of Sheared Model Decane. *J. Chem. Phys.* **1994**, *100* (1), 541. https://doi.org/10.1063/1.466970.
(61) Chen, T.; Smit, B.; Bell, A. T. Are Pressure Fluctuation-Based Equilibrium Methods Really Worse than Nonequilibrium Methods for Calculating Viscosities? *J. Chem. Phys.* **2009**, *131*

(24), 246101. https://doi.org/10.1063/1.3274802.
(62) Nosé, S.; Klein, M. L. Constant Pressure Molecular Dynamics for Molecular Systems. *Mol. Phys.* **1983**, *50* (5), 1055–1076. https://doi.org/10.1080/00268978300102851.
(63) Heyes, D. M. Pressure Tensor of Partial-Charge and Point-Dipole Lattices with Bulk and Surface Geometries. *Phys. Rev. B* **1994**, *49* (2), 755–764. https://doi.org/10.1103/PhysRevB.49.755.
(64) Galamba, N.; Nieto de Castro, C. A.; Ely, J. F. Molecular Dynamics Simulation of the Shear Viscosity of Molten Alkali Halides. *J. Phys. Chem. B* **2004**, *108* (11), 3658–3662. https://doi.org/10.1021/jp036234x.
(65) Galamba, N.; Nieto De Castro, C. A.; Ely, J. F. Shear Viscosity of Molten Alkali Halides from Equilibrium and Nonequilibrium Molecular-Dynamics Simulations. *J. Chem. Phys.* **2005**, *122* (22), 224501. https://doi.org/10.1063/1.1924706.
(66) Kabsch, W.; Sander, C. Dictionary of Protein Secondary Structure: Pattern Recognition of Hydrogen-Bonded and Geometrical Features. *Biopolymers* **1983**, *22* (12), 2577–2637. https://doi.org/10.1002/bip.360221211.
(67) Van Der Spoel, D.; Berendsen, H. J. Molecular Dynamics Simulations of Leu-Enkephalin in Water and DMSO. *Biophys. J.* **1997**, *72* (5), 2032–2041. https://doi.org/10.1016/S0006-3495(97)78847-7.
(68) Lipari, G.; Szabo, A. Model-Free Approach to the Interpretation of Nuclear Magnetic Resonance Relaxation in Macromolecules. 1. Theory and Range of Validity. *J. Am. Chem. Soc.* **1982**, *104* (17), 4546–4559. https://doi.org/10.1021/ja00381a009.
(69) Monteiro, H.; Paiva, A.; Duarte, A. R. C.; Galamba, N. On the Not so Anomalous Water-Induced Structural Transformations of Choline Chloride–Urea (Reline) Deep Eutectic System. *Phys. Chem. Chem. Phys.* **2023**, *25* (1), 439–454. https://doi.org/10.1039/D2CP04139A.
(70) Austin, R. H.; Beeson, K. W.; Eisenstein, L.; Frauenfelder, H.; Gunsalus, I. C. Dynamics of Ligand Binding to Myoglobin. *Biochemistry* **1975**, *14* (24), 5355–5373. https://doi.org/10.1021/bi00695a021.
(71) Fenimore, P. W.; Frauenfelder, H.; McMahon, B. H.; Young, R. D. Bulk-Solvent and Hydration-Shell Fluctuations, Similar to α- and β-Fluctuations in Glasses, Control Protein Motions and Functions. *Proc. Natl. Acad. Sci.* **2004**, *101* (40), 14408–14413. https://doi.org/10.1073/pnas.0405573101.
(72) Frauenfelder, H.; Fenimore, P. W.; Chen, G.; McMahon, B. H. Protein Folding Is Slaved to Solvent Motions. *Proc. Natl. Acad. Sci.* **2006**, *103* (42), 15469–15472. https://doi.org/10.1073/pnas.0607168103.
(73) Fenimore, P. W.; Frauenfelder, H.; McMahon, B. H.; Parak, F. G. Slaving: Solvent Fluctuations Dominate Protein Dynamics and Functions. *Proc. Natl. Acad. Sci.* **2002**, *99* (25), 16047–16051. https://doi.org/10.1073/pnas.212637899.
(74) Frauenfelder, H.; Chen, G.; Berendzen, J.; Fenimore, P. W.; Jansson, H.; McMahon, B. H.; Stroe, I. R.; Swenson, J.; Young, R. D. A Unified Model of Protein Dynamics. *Proc. Natl. Acad. Sci.* **2009**, *106* (13), 5129–5134. https://doi.org/10.1073/pnas.0900336106.
(75) Ansari, A.; Jones, C. M.; Henry, E. R.; Hofrichter, J.; Eaton, W. A. The Role of Solvent Viscosity in the Dynamics of Protein Conformational Changes. *Science* **1992**, *256* (5065), 1796–1798. https://doi.org/10.1126/science.1615323.
(76) Kramers, H. A. Brownian Motion in a Field of Force and the Diffusion Model of Chemical Reactions. *Physica* **1940**, *7* (4), 284–304. https://doi.org/10.1016/S0031-8914(40)90098-2.
(77) Jas, G. S.; Eaton, W. A.; Hofrichter, J. Effect of Viscosity on the Kinetics of α-Helix and β-Hairpin Formation. *J. Phys. Chem. B* **2001**, *105* (1), 261–272. https://doi.org/10.1021/jp0022048.
(78) Piana, S.; Lindorff-Larsen, K.; Shaw, D. E. Atomic-Level Description of Ubiquitin Folding. *Proc. Natl. Acad. Sci.* **2013**, *110* (15), 5915–5920. https://doi.org/10.1073/pnas.1218321110.

TOC